

The bottom-charmed meson spectrum from a QCD approach based on Tamm–Dancoff Approximation

L. M. Abreu*

*Instituto de Física, Universidade Federal da Bahia,
Campus Universitário de Ondina, Salvador, Bahia, 40170-115, Brazil*

F. M. da Costa Júnior†

*Instituto de Física, Universidade Federal da Bahia,
Campus Universitário de Ondina, Salvador, Bahia, 40170-115, Brazil and
Instituto Federal do Sertão Pernambucano, Petrolina, Pernambuco, Brazil*

A. G. Favero‡

Department of Physics, McGill University, Montréal, QC, H3A 2T8, Canada

Abstract

The bottom-charmed meson spectrum is studied in this work via an effective version of the Coulomb gauge QCD Hamiltonian. The Tamm-Dancoff approximation is employed to estimate the energies of the low-lying and radial-excited B_c states with quantum numbers $J^P = 0^-, 0^+, 1^-, 1^+, 2^+, 2^-$. In particular, we analyze the effects of incorporating an effective transverse hyperfine interaction and spin mixing. The Regge trajectories and hyperfine splitting of both S - and P -wave states are also examined. The numerical results are compared with available experimental data and theoretical predictions of other models.

*luciano.abreu@ufba.br

†francisco.miguel@ifsertao-pe.edu.br

‡aline.favero@mail.mcgill.ca

I. INTRODUCTION

Despite the enormous experimental developments on heavy-hadron physics in recent decades, bottom-charmed (B_c) spectroscopy remains much less known than the charmonium and bottomonium sectors. The reason comes from the fact that since the B_c is a quarkonium bound-state consisting of heavy-quarks with different flavors ($c\bar{b}$ or $b\bar{c}$), the production mechanism demands factories of $c\bar{c}$ and $b\bar{b}$ pairs, which results in a small production rate. On the other hand, the different quark-flavor content denies its annihilation into gluons, engendering uniquely weak decays for the pseudoscalar ground-state $B_c(1S)$ and hadronic or radiative transitions for excited states which are below the strong-decay BD threshold. These aspects suggest that B_c -states are more stable than their analogs in charmonium and bottomonium families, and therefore are pretty valuable to study heavy-quark dynamics and understand the dynamics of the strong interaction in a deeper level.

The first observation of B_c meson was performed by CDF Collaboration more than two decades ago [1], with the detection of the pseudoscalar ground-state $B_c(1S)^+$. It was confirmed later by other Collaborations [2, 3], and is the only state considered as an established particle with recognized quantum numbers, according to Particle Data Group (PDG) [4], with mass (6274.9 ± 0.8) MeV. The other state present in PDG with mass (6871.0 ± 1.7) MeV and identified as $B_c(2S)^+$ has its quantum numbers not confirmed. This is due to the controversy raised by the results from the ATLAS [5], CMS [6] and LHCb [7] Collaborations. ATLAS [5] reported the mass $(6842 \pm 4 \pm 5)$ MeV of an observed state consistent with a first radially excited pseudoscalar; while very recently CMS [6] and LHCb [7] detected two signals consistent with the 2^1S_0 and 2^3S_1 : for the 2^1S_0 the LHCb and CMS found the mass being respectively $(6872.1 \pm 1.3 \pm 0.1 \pm 0.8)$ MeV and $(6871.0 \pm 1.2 \pm 0.8 \pm 0.8)$ MeV. Besides, for the 2^3S_1 , LHCb obtained the mass $(6841 \pm 0.6 \pm 0.1 \pm 0.8)$ MeV, whereas CMS observed the mass difference $m[B_c(2^1S_0)] - m[B_c^*(2^3S_1)] = (29 \pm 1.5 \pm 0.7)$ MeV. Thus, it can be remarked two intriguing features from these reports. The first one is the apparent disagreement between the ATLAS and CMS, LHCb outcomes for the $B_c^*(2^3S_1)$ meson. One possible explanation is that the peak observed by ATLAS could be the superposition of the $B_c(2^1S_0)$ and $B_c^*(2^3S_1)$ states, quite narrowly spaced with respect to the resolution of the measurement. The second one is that the $B_c(2^1S_0)$ state emerges as heavier than the mass $B_c^*(2^3S_1)$, which is in conflict with theoretical estimations. The plausible justification

is that the observed $B_c^*(2S)$ peak has a mass lower than the true value, which remains unknown due to the impossibility of reconstruction of the low-energy photon emitted in the $B_c^{*+} \rightarrow B_c^+ \gamma$ [6]. Hence, more observations on B_c -meson family are expected in the nearest possible future in order to get a detailed characterization of heavy meson spectroscopy.

On theoretical grounds, different perspectives have been consecrated to investigate the B_c meson spectrum as well as to understand its properties. For example, it can be found studies in the context of non-relativistic quark models [8–16], relativistic constituent quark models [17–22], Quantum Chromodynamics (QCD) sum rules [23–25], lattice QCD [26–28] and Dyson-Schwinger and the Bethe-Salpeter equations approaches [29]. The point here is that this miscellany of distinct approaches produces a frame to be contrasted with available and future experimental results, which in the end makes possible a compelling comprehension of the B_c phenomenology.

That being so, the present study intends to contribute to the discussion and characterization of the B_c meson spectrum, by employing a different formalism with respect to the preceding analyses mentioned in the previous paragraph. The framework to be utilized is also known as Coulomb gauge QCD model [30–47]. This formulation is based on the exact QCD Hamiltonian in the Coulomb gauge, which is replaced by an effective Hamiltonian where the original non-perturbative confining and hyperfine interactions can be rearranged into calculable effective potentials between color densities as well as currents. The current quark and gluon field operators are dressed via Bogoliubov-Valatin method. This provides the possibility of using relativistic field theory and many-body techniques such as Tamm-Dancoff and Random Phase approximations. The vacuum is represented as a coherent BCS ground state with quark and gluon Cooper pairs (condensates), and the hadrons interpreted as quasiparticle excitations. This approach has been successfully applied to the description of properties of some types of light and heavy mesons, glueballs, gluelumps, hybrids and tetraquarks [30–47]. So, these reports demonstrate that this model is efficient in retrieving the essential aspects of QCD with a minimal number of free parameters (current quark masses and dynamical constants) and yielding reasonable predictions.

Here we extend the range of applications of the Coulomb gauge QCD model by studying the basic features of B_c mesons within an unified scheme. The interactions between quarks and antiquarks will be treated through an improved confining potential and a transverse hyperfine interaction, whose kernel is a Yukawa-type potential. Estimations for the energies of

the low-lying and radial-excited B_c states with quantum numbers $J^P = 0^-, 0^+, 1^-, 1^+, 2^+, 2^-$ are obtained. Also, the Regge trajectories are constructed, and a discussion about the hyperfine splittings of the S - and P -wave spectroscopy is done. The comparison of our results with other works is performed as well.

The paper is organized as follows. In Section II, we present the Coulomb gauge QCD model within Tamm-Dancoff approximation. Section III is devoted to show and analyze the numerical calculations of the bottom-charmed meson spectrum, the Regge trajectories and the hyperfine splittings. Concluding remarks are in Section IV. In Appendix we present explicitly the B_c meson spin-orbital wave functions and kernels of the TDA equation of motion used.

II. THE MODEL

Let us start by introducing the formalism to be used in the analysis of the B_c meson spectrum. It is a Coulomb gauge QCD-inspired model, whose effective Hamiltonian is given by [32–38, 41, 42, 46, 47],

$$H_{eff} = \int d\mathbf{x} \Psi^\dagger(\mathbf{x}) [-i\boldsymbol{\alpha} \cdot \boldsymbol{\nabla} + \beta m] \Psi(\mathbf{x}) + H_C + H_T, \quad (1)$$

where Ψ and m are the current quark field and mass, respectively. The terms H_C and H_T are the effective couplings associated to the Coulomb and quark hyperfine interactions, i.e.

$$\begin{aligned} H_C &= -\frac{1}{2} \int d\mathbf{x} d\mathbf{y} \rho^a(\mathbf{x}) \hat{V}(|\mathbf{x} - \mathbf{y}|) \rho^a(\mathbf{y}), \\ H_T &= \frac{1}{2} \int d\mathbf{x} d\mathbf{y} J_i^a(\mathbf{x}) \hat{U}_{ij}(\mathbf{x}, \mathbf{y}) J_j^a(\mathbf{y}), \end{aligned} \quad (2)$$

where $\rho^a(\mathbf{x}) = \Psi^\dagger(\mathbf{x}) T^a \Psi(\mathbf{x})$ are the color densities and $\mathbf{J}^a(\mathbf{x}) = \Psi^\dagger(\mathbf{x}) \boldsymbol{\alpha} T^a \Psi(\mathbf{x})$ the quark color currents, with T^a ($a = 1, 2, \dots, 8$) being the $SU_c(3)$ generators. In the equations above the flavor indices are not explicitly displayed to simplify the notation. Also, it should be mentioned that pure gluonic contributions have been excluded due to the fact that our interest is devoted to the $q\bar{q}$ states.

We write down below the kernels of the effective couplings in Eq. (2) used in the calculations. For the Coulomb longitudinal interaction H_C , the kernel is assumed to be an

improved confining potential based on Yang-Mills dynamics, which in momentum space is represented as [36],

$$V(p) = \begin{cases} \left(-12.25 \frac{m_g^{1.93}}{p^{3.93}}\right), & p < m_g, \\ -\frac{8.07 \ln\left(\frac{p^2}{m_g^2} + 0.82\right)^{-0.62}}{p^2 \ln\left(\frac{p^2}{m_g^2} + 1.41\right)^{0.8}}, & p > m_g, \end{cases} \quad (3)$$

where m_g is a parameter. Although we are not directly dealing with dynamical gluons in our model, we interpret them as responsible for $V(p)$, obtained from a self-consistent method of the nonabelian degrees of freedom in the presence of static quarks, as noticed by the authors of Ref. [33]. Viewed in this way, m_g can be interpreted as a dynamical mass scale for the constituent gluons.

Turning to the term H_T , it is associated to the quark hyperfine interaction of type $\vec{\alpha} \cdot \vec{\alpha}$ from the second-order coupling between quarks and transverse gluons after integrating out gluonic degrees of freedom. In this sense, the effective transverse hyperfine potential carries the kernel \hat{U}_{ij} which keeps the structure of transverse gauge condition,

$$\hat{U}_{ij}(\mathbf{x}, \mathbf{y}) = \left(\delta_{ij} - \frac{\nabla_i \nabla_j}{\nabla^2}\right)_{\mathbf{x}} \hat{U}(|\mathbf{x} - \mathbf{y}|), \quad (4)$$

with \hat{U} being chosen to mimic one-gluon exchange potential. Following the analysis done in Ref. [36], in which a Yukawa-type potential appears as the preferred one for reasonable meson descriptions, we choose

$$U(p) = C_h \begin{cases} (-24.57) \frac{1}{p^2 + m_g^2}, & p < m_g, \\ -\frac{8.07 \ln\left(\frac{p^2}{m_g^2} + 0.82\right)^{-0.62}}{p^2 \ln\left(\frac{p^2}{m_g^2} + 1.41\right)^{0.8}}, & p > m_g, \end{cases} \quad (5)$$

with the constant C_h standing for the global strength, and the factor (-24.57) being determined by matching the high and low momentum ranges at the scale m_g .

Next, we apply an appropriate quark basis in which calculations for meson states are most conveniently made. Following the standard Bogoliubov-Valatin method (see for example Ref. [34]), we perform the Bogoliubov transformation from the current quark basis

to a improved quasiparticle quark basis represented by quasiparticle and antiquasiparticle $B_{\lambda c}^{(\dagger)}(\mathbf{k})$, $D_{\lambda c}^{(\dagger)}(\mathbf{k})$ operators, which allows us to write the quark field as

$$\Psi(\mathbf{x}) = \sum_{\lambda i} \int \frac{d^3 k}{(2\pi)^3} \left[\mathcal{U}_\lambda(\mathbf{k}) B_{\lambda i}(\mathbf{k}) + \mathcal{V}_\lambda(-\mathbf{k}) D_{\lambda i}^\dagger(-\mathbf{k}) \right] e^{i\mathbf{k}\cdot\mathbf{x}} \hat{\mathbf{e}}_i, \quad (6)$$

where λ and i denote the helicity and color indices ($i = 1, 2, 3$), respectively; $\{\hat{\mathbf{e}}_c\}$ is the color vector basis; \mathcal{U} and \mathcal{V} are Dirac spinors forming a complete basis,

$$\mathcal{U}_\lambda(\mathbf{k}) = \frac{1}{\sqrt{2}} \begin{pmatrix} \sqrt{1 + \sin \phi(k)} \chi_\lambda \\ \sqrt{1 - \sin \phi(k)} \boldsymbol{\sigma} \cdot \hat{\mathbf{k}} \chi_\lambda \end{pmatrix}, \quad (7)$$

$$\mathcal{V}_\lambda(-\mathbf{k}) = \frac{1}{\sqrt{2}} \begin{pmatrix} -\sqrt{1 - \sin \phi(k)} \boldsymbol{\sigma} \cdot \hat{\mathbf{k}} i\sigma_2 \chi_\lambda \\ \sqrt{1 + \sin \phi(k)} i\sigma_2 \chi_\lambda \end{pmatrix}, \quad (8)$$

with χ_λ being the Pauli spinors.

The Bogoliubov angle $\phi(|\mathbf{k}|) \equiv \phi_k$ connecting the current and quasiparticle quark bases is obtained by the variational minimization of the quasiparticle vacuum energy $\delta \langle \Omega | H | \Omega \rangle = 0$, yielding the gap equation

$$k s_k - m c_k = \int_0^\infty \frac{q^2}{6\pi^2} [s_k c_q (V_1 + 2W_0) - s_q c_k (V_0 + U_0)], \quad (9)$$

where the functions $s_k \equiv \sin \phi_k$ and $c_k \equiv \cos \phi_k$ are related to the running quark mass $M(k)$ through the relationship $M(k) = k \tan \phi_k$. We identify $M(k) \rightarrow m$ at high k , while at low k the constituent quark mass is extracted, $M(0) \rightarrow \mathcal{M}$. The functions V_0, V_1 and U_0 denote angular integrals of longitudinal and transverse potentials in the form

$$F_n(k, q) \equiv \int_{-1}^1 dx x^n F(|\mathbf{k} - \mathbf{q}|), \quad (10)$$

with $x = \hat{k} \cdot \hat{q}$; and the W -function is defined as

$$W(|\mathbf{k} - \mathbf{q}|) \equiv U(|\mathbf{k} - \mathbf{q}|) \frac{x(k^2 + q^2) - kq(1 + x^2)}{|\mathbf{k} - \mathbf{q}|^2}. \quad (11)$$

Also, the expectation value of the effective Hamiltonian with respect to the one-quasiparticle state $|q\rangle \equiv B_{ac}^\dagger(\mathbf{k}) |\Omega\rangle$ engenders the expression that can be identified as the self-energy of the quasiparticle,

$$\begin{aligned} \epsilon_k &= \langle q | H_{eff} | q \rangle \\ &= m s_k + k c_k - \int_0^\infty \frac{q^2}{6\pi^2} [s_k s_q (V_0 + 2U_0) + c_k c_q (V_1 + W_0)]. \end{aligned} \quad (12)$$

It must be observed that a meson in this framework is supposed to be an excited state consisting of a bound state of the quasiparticle and antiquasiparticle. Then, it is useful to introduce the meson creation operator in the TDA scheme, which is a bosonization method that has been revealed to be a good approximation for a large number of meson families, excluding only the case of the pions. Accordingly, the quasiparticle–antiquasiparticle operator is given by

$$Q_{nJP}^\dagger = \sum_{\lambda\lambda'} \int \frac{d\mathbf{k}}{(2\pi)^3} \Psi_{\lambda\lambda'}^{(nJP)}(\mathbf{k}) B_\lambda^\dagger(\mathbf{k}) D_{\lambda'}^\dagger(-\mathbf{k}), \quad (13)$$

where $\Psi_{\alpha\beta}^{(nJP)}$ means the wavefunction corresponding to an open-flavor meson state with total angular momentum J , parity P and radial quantum number n (we have omitted the color and flavor indices).

Now the method of calculating the energy levels of mesonic bound states can be expressed. The energies are obtained via the TDA equation of motion for an open-flavor meson, defined by

$$\langle \Psi^{(nJP)} | [H_{eff}, Q_{nJP}^\dagger] | \Omega \rangle = (E_{nJP} - E_0) \langle \Psi^{(nJP)} | Q_{nJP}^\dagger | \Omega \rangle. \quad (14)$$

This equation can be recast into a more convenient form, by profiting from the rotational invariance of H_{eff} and constructing the wavefunctions via multiplication of Pauli σ matrices by powers of orbital momentum \hat{k}^l to get partial waves. Concerning this last procedure, we indicate to the reader the Appendix A of Ref. [46], in which the specific case of axial mesons is discussed. Notwithstanding, for completeness we express in detail the wavefunctions exploited in this work, which can be written as (again omitting the flavor indices):

$$\Psi_{\lambda\lambda'}^{(nJP)}(\mathbf{k}) = \frac{\delta_{ij}^{(\text{color})}}{\sqrt{3}} R^{(nJP)}(k) \psi_{\lambda\lambda'}^{(JP)}(\mathbf{k}), \quad (15)$$

where $R^{(nJP)}(k)$ is the radial wavefunction; $\psi_{\lambda\lambda'}^{(JP)}(\mathbf{k})$ carries the angular-momentum dependence, and assumes a distinct form according to the nature of the meson state described by the quantum numbers L, S, J , which specify the parity $P = (-1)^{L+1}$ and also the charge conjugation $C = (-1)^{L+S}$, if the quark and antiquark have the opposite flavor (equal mass). These wavefunctions are given explicitly in Appendix A. After that, we perform the diagonalization of the effective Hamiltonian in the TDA representation, which is undertaken by the computation of the trace of spinor products coming from commutators in the left-hand

side of Eq. (14). The final expression for the TDA equation of motion is

$$M_{nJP} R^{(nJP)}(k) = (\epsilon_k^b + \epsilon_k^c) R^{(nJP)}(k) + \int_0^\infty \frac{q^2 dq}{12\pi^2} K^{(JP)}(k, q) R^{(nJP)}(q), \quad (16)$$

where $M_{nJP} \equiv E_{nJP} - E_0$ is the energy of the B_c meson state; $\epsilon_k^b(\epsilon_k^c)$ is the self-energy of the (anti)quasiparticle associated to the $b(c)$ quark; and $K^{(JP)}(k, q)$ is the kernel bearing the potential terms, which is dependent on the meson quantum numbers. We should remark that several versions of kernels are accessible in literature, written using different basis as well as distinct interaction terms. Until now, the tensor cases with both longitudinal and transverse potentials, however, are not available (at least to our knowledge). In view of these considerations, the relevant kernels obtained for the mesons described by the wavefunctions given by Eqs. (A1)-(A8) are expressed in Appendix B (Eqs. (B2)-(B8)).

As a final comment in this Section, we must note that open-flavor mesons, like the B_c mesons, are not eigenstates of charge conjugation, since they have the quark and antiquark with different flavor. Therefore, the total spin (S) is no longer a good quantum number, and spin-singlet and spin-triplet states with $J = L$ can mix. This is the case of axial (n^3P_1 and n^1P_1) and pseudotensor (n^3D_2 and n^1D_2) states reported above. A simple mixing prescription for these $J = L$ states is:

$$\begin{aligned} |nL'_L\rangle &= \cos\theta_{nL}|n^1L_L\rangle + \sin\theta_{nL}|n^3L_L\rangle, \\ |nL_L\rangle &= -\sin\theta_{nL}|n^1L_L\rangle + \cos\theta_{nL}|n^3L_L\rangle, \end{aligned} \quad (17)$$

where θ_{nL} is the mixing angle and nL'_L, nL_L are the physical states. Supposing that the masses of b and c -quarks satisfy the limit $m_b \gg m_c$, this leads to the extreme heavy-light expression: $\theta_{nL} \rightarrow \tan^{-1}\sqrt{L/(L+1)}$, giving $\theta_{nP} \rightarrow 35.3^\circ, \theta_{nD} \rightarrow 39.2^\circ$. Here we adopt the following relation between the masses of $(n^3L_L - n^1L_L)$ and $(nL'_L - nL_L)$ pairs [48],

$$\begin{aligned} M(nL_L) &= M(n^1L_L) \cos^2\theta_{nL} + M(n^3L_L) \sin^2\theta_{nL} - [M(n^3L_L) - M(n^1L_L)] \frac{\sin^2 2\theta_{nL}}{2 \cos 2\theta_{nL}}, \\ M(nL'_L) &= M(n^1L_L) \sin^2\theta_{nL} + M(n^3L_L) \cos^2\theta_{nL} + [M(n^3L_L) - M(n^1L_L)] \frac{\sin^2 2\theta_{nL}}{2 \cos 2\theta_{nL}}. \end{aligned} \quad (18)$$

III. NUMERICAL RESULTS

In this Section are exhibited the results for the spectrum of the B_c mesons, generated with the model sketched out above. Briefly, the strategy consists in solving the gap equation (Eq. (9)) for each flavor, in order to get the k -dependent gap angles ϕ_k^b and ϕ_k^c ; they supply the values of functions $c_{k(q)}^{b(c)}$ and $s_{k(q)}^{b(c)}$ to generate M_{nJP} that solve numerically the TDA equation of motion in Eq. (16). It should be emphasized the adoption in the calculations of kernels with interactions represented by an improved confining potential and a transverse Yukawa-type potential playing the role of the exchange of a constituent gluon.

In the Coulomb gauge QCD model the input parameters to be fitted to the experimental data are the dynamical mass of the constituent gluon m_g , the current quark masses of the b and c quarks, m_b and m_c , and the magnitude of the transverse potential C_h . However, as discussed in the Introduction, data for the B_c -meson families are scarce at present, despite recent results from the ATLAS [5], CMS [6] and LHCb [7] Collaborations. According to PDG [4], until now there are two B_c mesons observed: the ground pseudoscalar state is the only one considered as an established particle, with mass $M[B_c(1S)^+] \approx (6274.9 \pm 0.8)$ MeV; the other one with mass (6871.0 ± 1.7) MeV is consistent with a first radially excited pseudoscalar, but quantum numbers are not confirmed. Nevertheless, it should be also mentioned that ATLAS and LHCb Collaborations reported the observations of peaks at $(6842 \pm 4 \pm 5)$ MeV and $(6841 \pm 0.6 \pm 0.1 \pm 0.8)$ MeV, respectively, which are consistent with the $B_c^*(2^3S_1)$. Remarking that the goal here is to extract the basic picture of the B_c meson spectrum, the values of the parameters (m_b, m_c, m_g, C_h) are adjusted to reproduce approximately these reported states, in particular the confirmed $B_c(1S)^+$.

We start by showing in Table I the values of constituent quark masses $\mathcal{M}_{b,c}$ engendered by the current quark masses $m_b = 4000$ MeV, $m_c = 950$ MeV used as inputs in this subsection. The remaining parameters C_h and m_g are taken with different but near values in order to evaluate their impact on the constituent quark masses $\mathcal{M}_{b,c}$, extracted from the limit $M_{b,c}(k \rightarrow 0) \equiv \mathcal{M}_{b,c}$. They are chosen obviously keeping in mind the range that better matches the physical states. It can be seen that the growth of C_h and m_g yields greater values of $\mathcal{M}_{b,c}$, because of the modification of the gap angles coming from solutions of the gap equation. We stress that the values of current and constituent quark masses are smaller than in some quark models, due to the contributions from interaction potentials

in gap equation (9) and in the self-energy $\epsilon_k^{b,c}$ (Eq. (12)). For a detailed discussion we refer the reader to Refs. [36, 46]. On this regard, it deserves to be cited that very recent ($n_f = 2 + 1 + 1$)–lattice QCD calculations obtained estimations for the charm quark mass by about 980-995 MeV [49, 50], which are close to the one we utilize.

TABLE I: The constituent quark masses $\mathcal{M}_{b,c}$ engendered by the current quark masses $m_b = 4000$ MeV, $m_c = 950$ MeV used as inputs in this subsection. $\mathcal{M}_{b,c}$ are obtained from the gap angles ϕ_k^b and ϕ_k^c that solve the gap equation (Eq. (9)), through the relationship $\lim_{k \rightarrow 0} M_{b,c}(k) = \lim_{k \rightarrow 0} k \tan \phi_k^{b,c} \equiv \mathcal{M}_{b,c}$. The column “Set” denotes the set of parameters (m_g, C_h) used. All quantities are given in MeV, except the value of C_h , which is adimensional.

Set (m_g, C_h)	\mathcal{M}_c	\mathcal{M}_b
I (600, 0.4)	1208	4343
II (650, 0.4)	1222	4362
III (700, 0.4)	1236	4380
IV (700, 0.5)	1288	4452
Other estimates [4, 49, 50]	1000-1600	4600-5100

For the sake of completeness, we briefly discuss the overall momentum-dependence of the Bogoliubov angles for the different flavors obtained from the solutions of the gap equation (Eq. (9)). To this end, in Fig. 1 the solutions ϕ_k^b and ϕ_k^c are plotted as a function of k . At higher values of k , the solutions exhibit a decreasing exponential behavior, with the c -flavor case experiencing a faster lessening. Particularly, the obtention of $\phi_k^{b,c} \rightarrow 0$ in the limit $k \rightarrow \infty$ implies the finiteness of the vacuum energy. At small values of k , the solutions present a linear behavior with a negative slope and a sharp peak, yielding $\phi_k^{b,c} \rightarrow \pi/2$ at $k \rightarrow 0$, which also assures the finite-energy density of the vacuum. Although the specific curves for $\phi_k^{b,c}$ obviously depend on the potentials and parameters considered, the point to be stressed is that this formalism yields well-behaved solutions of the gap equation that will be used as inputs in the obtention of the meson spectrum.

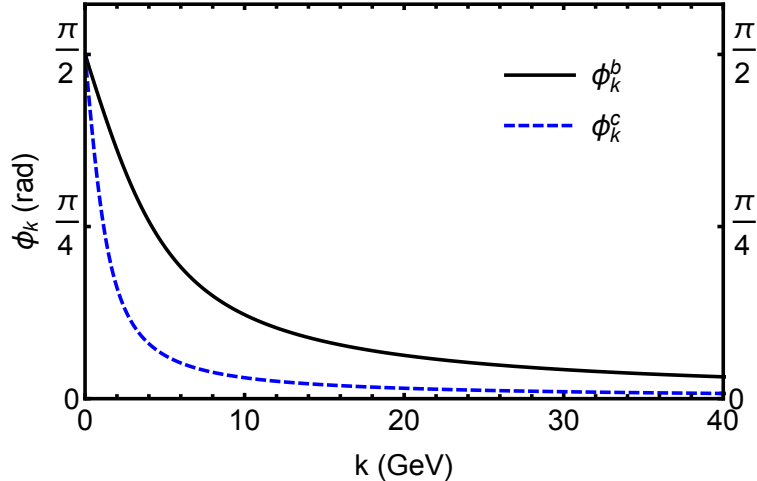


FIG. 1: Bogoliubov angles ϕ_k^b and ϕ_k^c , obtained from the solutions of the gap equation (Eq. (9)), as a function of the modulus of the momentum (k). We have used the current quark masses $m_b = 4000$ MeV, $m_c = 950$ MeV and the set III for the parameters (m_g, C_h) , in conformity with Table I.

A. Mass Spectrum

Now we report our predictions for the energy levels for the B_c states, extracted from the numerical solutions of the TDA equation in Eq. (16) considering the different quantum numbers. In Table II are listed the computed masses for ground and radially excited states of $b\bar{c}$ considering the different sets of input parameters of Table I. It gives an overall view of the behavior of computed masses as the parameters C_h and m_g change. In the region of parameter space considered, the augmentation of constituent gluon mass by 100 MeV increases the estimates by about 100-200 MeV, as well as the strengthening of magnitude of transverse potential by 0.1 yields greater masses by about 100-150 MeV.

TABLE II: TDA masses of lowest-lying and radially excited B_c states, obtained for $m_c = 950$ MeV and $m_b = 4000$ MeV. The column “Set” denotes the set of parameters (m_g, C_h) used in conformity with Table I. The masses are given in MeV. Our calculated masses are rounded to 1 MeV. The mixing angles used are: $\theta_{1P} - \theta_{5P} = 35.3^\circ, \theta_{1D} = 42.5^\circ, \theta_{2D} = 42.2^\circ, \theta_{3D} = 33.2^\circ, \theta_{4D} = 21.1^\circ, \theta_{5D} = 5.2^\circ$. The results that better fit to the observed states are in boldface.

State (J^P)	Set	E_1	E_2	E_3	E_4	E_5
0^-	I	6146	6619	6986	7298	7573
	II	6212	6733	7136	7477	7779
	III	6277	6845	7284	7656	7983
	IV	6417	6977	7411	7779	8103
0^+	I	6449	6852	7187	7478	7740
	II	6545	6989	7356	7675	7961
	III	6639	7123	7523	7871	8181
	IV	6786	7264	7659	8002	8309
1^-	I	6154	6625	6990	7302	7576
	II	6222	6739	7141	7482	7782
	III	6288	6853	7290	7661	7988
	IV	6431	6986	7418	7785	8108
1^+	I	6423	6821	7153	7443	7703
	II	6516	6955	7318	7635	7920
	III	6606	7088	7488	7836	8148
	IV	6744	7216	7608	7950	8254
$1^{+'}$	I	6456	6845	7171	7458	7715
	II	6552	6979	7339	7653	7935
	III	6.656	7121	7513	7856	8164
	IV	6783	7243	7629	7968	8272

2^+	I	6468	6853	7178	7463	7720
	II	6568	6991	7347	7659	7940
	III	6667	7127	7515	7854	8159
	IV	6805	7259	7641	7976	8277
2^-	I	6687	7023	7331	7600	7845
	II	6812	7177	7512	7808	8076
	III	6931	7334	7694	8015	8306
	IV	7046	7441	7815	8135	8422
$2^{-'}$	I	6687	7043	7338	7608	7853
	II	6801	7197	7522	7816	8085
	III	6920	7345	7704	8024	8315
	IV	7068	7492	7828	8144	8432

On experimental grounds, the set of parameters III seems to generate findings that better fit to the observed states. Although fine tuning of the parameters can give even better outcomes, we believe that set III seems sufficient to generate findings in good conformity with observed states. The spectrum generated for this set is shown schematically in Fig. 2.

It is also noteworthy to evaluate our predictions in light of other works existent in the literature. To this end, in Table III our calculated B_c masses with the set of parameters III are compared with other theoretical results and available experimental data. Stated explicitly, the theoretical frameworks employed in these other studies are: relativized constituent quark model with the presence of a linear confining potential and a color Coulomb interaction [17]; constituent quark model in heavy quark symmetry limit with scalar confining and vector Coulomb potentials [18]; non-relativistic quark model (NRQM) consisting of a confinement potential and one gluon exchange potential [9]; nonrelativistic linear potential model with a spin-dependent interaction [14].

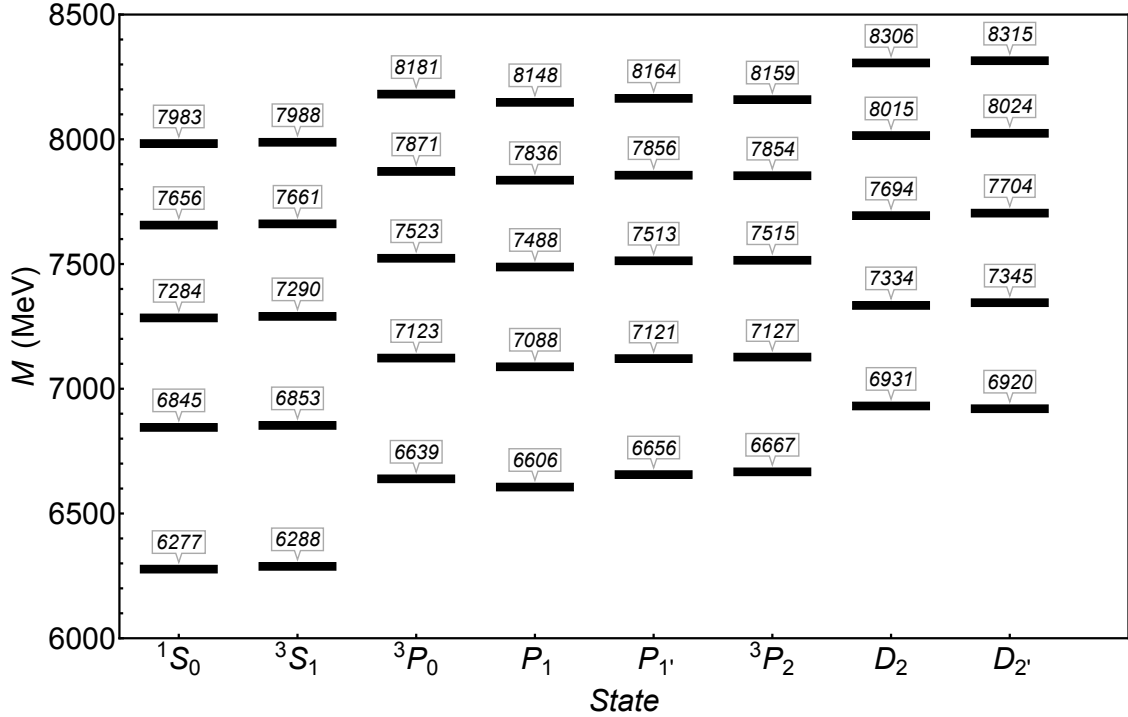


FIG. 2: B_c spectrum generated for the set of parameters III.

TABLE III: Last Column: TDA masses of lowest-lying and radially excited B_c states obtained for the set of parameters III in Table I. Other columns: predictions of other works existent in the literature and available experimental data. The $B_c(1^1S_0)$ is the only established particle and its mass has been taken from PDG [4]. The states observed by ATLAS [5], CMS [6] and LHCb [7] are not considered as well-established by PDG; quantum numbers of the so-called 2^1S_0 need to be confirmed. The masses are given in MeV.

State	J^P	Ref. [17]	Ref. [18]	Ref. [9]	Ref. [12]	Ref. [14]	Exp. Data (*[5]; †[6]; ‡[7])	Our Results (Set III)
$B_c(1^3S_1)$	1^-	6338	6340	6357	6314	6326	...	6288
$B_c(1^1S_0)$	0^-	6271	6260	6275	6274	6271	6275 (PDG)	6277
$B_c(2^3S_1)$	1^-	6887	6900	8697	6855	6890	6842 [†] ; 6841 [‡]	6853

$B_c(2^1S_0)$	0^-	6855	6850	6862	6841	6871	6842*; 6871 [†] ; 6872 [‡]	6845
$B_c(3^3S_1)$	1^-	7272	7280	7333	7206	7252	...	7290
$B_c(3^1S_0)$	0^-	7250	7240	7308	7197	7239	...	7284
$B_c(1^3P_2)$	2^+	6768	6760	6737	6753	6787	...	6667
$B_c(1P'_1)$	1^+	6750	6740	6734	6744	6776	...	6656
$B_c(1P_1)$	1^+	6741	6730	6686	6725	6757	...	6606
$B_c(1^3P_0)$	0^+	6706	6680	6638	6701	6714	...	6639
$B_c(2^3P_2)$	2^+	7164	7160	7175	7111	7160	...	7127
$B_c(2P'_1)$	1^+	7150	7150	7173	7098	7150	...	7121
$B_c(2P_1)$	1^+	7145	7140	7137	7105	7134	...	7088
$B_c(2^3P_0)$	0^+	7122	7100	7084	7086	7107	...	7123
$B_c(3^3P_2)$	2^+	...	7480	7575	7406	7464	...	7515
$B_c(3P'_1)$	1^+	...	7470	7572	7393	7458	...	7513
$B_c(3P_1)$	1^+	...	7460	7546	7405	7441	...	7488
$B_c(3^3P_0)$	0^+	...	7430	7492	7389	7420	...	7523
$B_c(1D'_2)$	2^-	7036	...	7003	6984	7032	...	6920
$B_c(1D_2)$	2^-	7041	...	6974	6986	7024	...	6931
$B_c(2D'_2)$	2^-	7408	7293	7347	...	7345
$B_c(2D_2)$	2^-	7385	7294	7343	...	7334
$B_c(3D'_2)$	2^-	7783	7562	7623	...	7704
$B_c(3D_2)$	2^-	7781	7563	7620	...	7694

We stress that our findings, specially for $B_c(1S)$ and $B_c^*(2S)$, present a very good fit with the measured data when the experimental errors are bore in mind. But this comparison must be done with care, because the observed $B_c^*(2S)$ peak has a mass lower than the true value, which remains unknown due to the impossibility of reconstruction of the low-energy photon emitted in the $B_c^{*+} \rightarrow B_c^+\gamma$, as pointed out in Ref. [6]. Moreover, the mass of the first radial excitation $B_c(2S)$ is heavier than the ground state $B_c(1S)$ by about 557 MeV, which is fairly good in light of experimental observations, keeping the fact that $B_c(2S)$ is not yet well-established according to PDG [4].

Furthermore, it can be seen that our outcomes get the B_c spectrum in reasonable concordance with other potential model predictions. In general, the masses predicted by us for the low-lying states have a difference with respect to previous works ranging from a few MeV up to tens of MeV. The exceptions having larger mass deviations are the $1^3P_2, 1P_1, 1P_1'$ states. For higher mass states, bigger discrepancies among the predictions are evident, but most of our results are between the lower and upper values reported in Table II. Particularly, our results for $1S, 2S, 3S, 2P$ -wave states are up to a few tens of MeV discrepant with those with relativized constituent quark model from Ref. [17], while for $1P_2, 1P_1^{(\prime)}, 1D$ -wave states are about 100 – 140 MeV smaller.

B. Regge Trajectories

In addition, the energy levels listed in Tables II and III allow us to obtain the mass relation between the ground states and their radial and angular excited states, and therefore construct the Regge trajectories in the (n, M^2) and (J, M^2) planes. They are then plotted in Fig. 3. In these plots, we assume that the Regge slopes are independent of charge conjugation, in accordance with the C -invariance of QCD [51], and also that the slopes of the parity partner trajectories coincide.

It can be remarked that the behavior of squared masses with radial quantum number and J^P (top and middle panels) is not exactly linear. This fact is clearly pronounced in (n, M^2) plane, due to the high excitation number. More precisely, the daughter trajectories (incorporating both radially and orbitally excited states) manifest extrapolations closer to a linear fit. However, the parent trajectories (beginning from the ground states) reveal a nonlinear nature, mostly in the region of smaller mass. This is in qualitative accordance with other works that investigated heavy quarkonia states; see for instance Refs. [51–55]. Notwithstanding, using the linear approximation for the Regge trajectories through the laws [52, 56–58],

$$\begin{aligned} M^2(J) &= \alpha_0\beta + J\alpha, \\ M^2(n) &= \beta_0 + n\beta, \end{aligned} \tag{19}$$

where α_0, β_0 are the intercepts and α, β the slopes of each corresponding trajectory on which the meson lies. Now applying this hypothesis in our scenario we can extract the

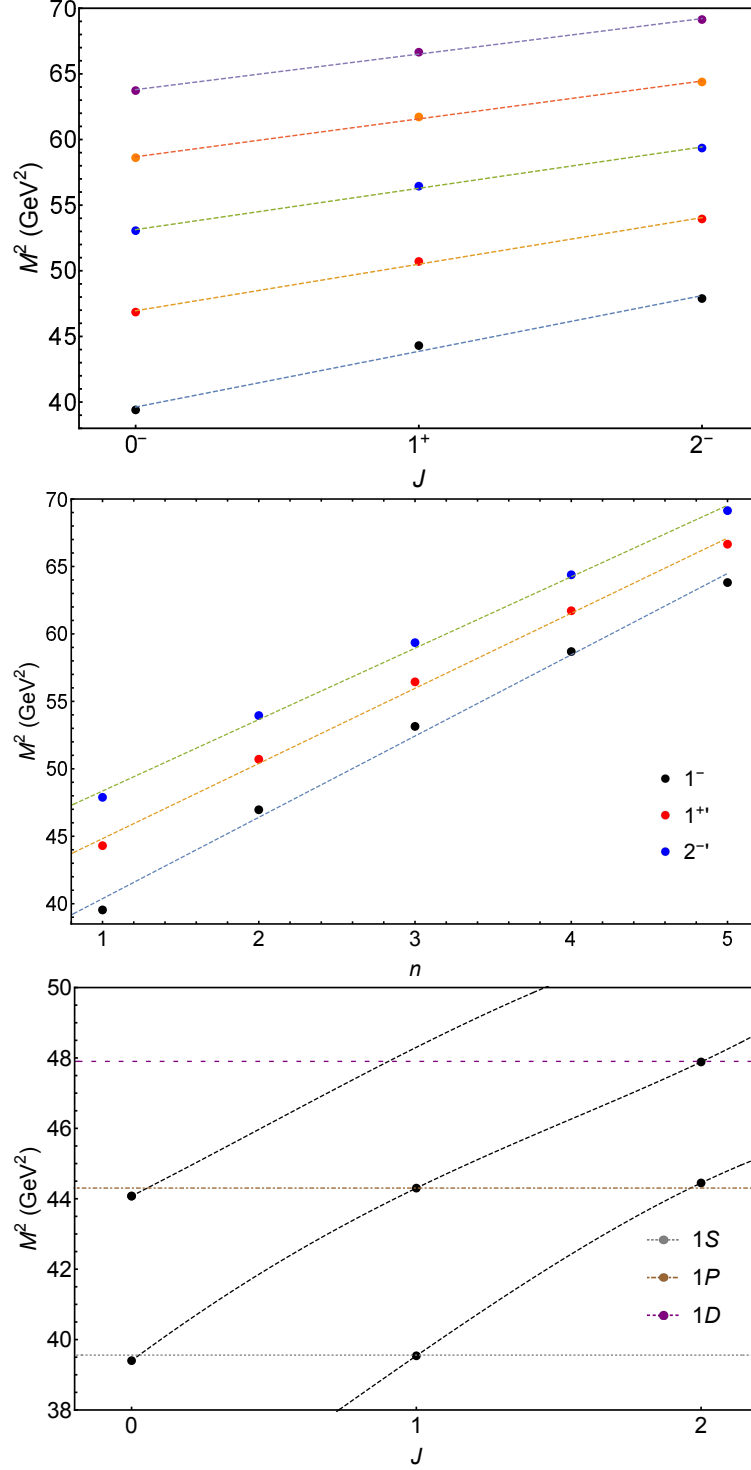


FIG. 3: Top Panel: Parent and Regge trajectories in (J, M^2) plane for B_c states with unnatural parity $P = (-1)^J$, for $n = 1, \dots, 5$ (from bottom to top). Middle Panel: Regge trajectories in (n, M^2) plane for S -wave vector, P -wave vector and D -wave tensor B_c states. Bottom Panel: Nonlinear trajectories in (J, M^2) plane starting from vector, pseudoscalar and scalar B_c states (from bottom to top), with lines indicating the regions of $1S, 1P, 1D$ states. Circles represent the predicted masses shown in Table II, taking the γ values of the set of parameters III.

parameters $\alpha_0, \beta_0, \alpha, \beta$ from the linear fits displayed in the top and middle panels of Fig. 3. The estimated values are listed in Table IV. These results are in reasonable accordance with the existing literature, when compared for example with Ref. [52].

TABLE IV: Fitted parameters for the linear fit in Eq. (19) of parent and daughter Regge trajectories in the top and middle panels of Fig. 3. The quantities are given in GeV^2 .

(J, M^2) plane		
Trajectory	α_0	α
Parent	39.620	4.243
1st Daughter	46.956	3.548
2nd Daughter	53.137	3.147
3rd Daughter	58.689	2.885
4th Daughter	63.801	2.705
(n, M^2) plane		
State	β_0	β
1^-	34.349	6.027
$1^{+'}$	39.253	5.570
2^-	43.060	5.294

C. Hyperfine splittings

Additionally, another relevant feature to be noticed is the hyperfine splitting of B_c states. We start with S -wave states. The hyperfine splittings Δ_{nS}^{HFS} are listed in Table V for the set of parameters III chosen as well as other sets in order to see the influence of their change. Despite the small values obtained for these sets, as expected these splittings decrease for higher excited states, and get larger as the parameter C_h grows. Our calculations yield the mass for $B_c(2S)$ heavier than for $B_c^*(2S)$, which coincides with the other theoretical expectations. Nonetheless, our estimations engenders smaller $\Delta_{2S}^{HFS} = M(2^3S_1) - M(2^1S_0)$ hyperfine splitting, as already remarked in Table V, but not too different from the finding

in Ref. [14].

TABLE V: The hyperfine splittings for the B_c system states, obtained for the set of parameters in Table I. We use the respective definition for the hyperfine splitting: $\Delta_{nS}^{HFS} = M(n^3S_1) - M(n^1S_0)$. The set used in Table III is in boldface. The quantities are given in MeV.

Set	Δ_{1S}^{HFS}	Δ_{2S}^{HFS}	Δ_{3S}^{HFS}	Δ_{4S}^{HFS}	Δ_{5S}^{HFS}
I	8	6	4	4	3
II	10	6	5	5	3
III	11	8	6	5	5
IV	14	9	7	6	5

Now we devote our attention to the hyperfine splitting of the P -wave states. For a systematic discussion of the hyperfine splitting for P -wave states in the context of hidden-flavor quarkonia, see for example Ref. [59]. In the case of bottom-charmed quarkonia, let us follow as motivation the discussion done in Ref. [15]. Experimentally, it can be remarked that the spin-singlet P -wave states almost coincide with the spin-averaged centroid of the triplet [4] for $c\bar{c}$ and $b\bar{b}$ systems, yielding ideally

$$E(n^1P_1) = \frac{1}{9} [5E(n^3P_2) + 3E(n^3P_1) + E(n^3P_0)]. \quad (20)$$

Since for the B_c system the C -parity is no longer a good quantum number, the states $n^3P_1 - n^1P_1$ can mix according to Eq. (17), and therefore Eq. (20) cannot be directly used. Nevertheless, assuming that the relation $E(n^3P_1) \approx E(n^1P_1)$ holds for B_c mesons, then Eq. (20) gives [60]

$$E(n^3P_0) + 5E(n^3P_2) = 3[E(nP_1) + E(nP'_1)]. \quad (21)$$

In order to test the validity of the relation above, the ratio among the masses can be introduced [15]:

$$r = \frac{E(n^3P_0) + 5E(n^3P_2)}{3[E(nP_1) + E(nP'_1)]}. \quad (22)$$

So, the deviation from $r = 1$ accounts for how much Eq. (21) is being violated. In this way, the estimations of r for our calculations reported above are listed in Table VI. We see that the relative theoretical errors for the lowest-lying and radially-excited states are below 0.5%, being even smaller for the excited states. Thus, the relation in Eq. (21) holds to a fair precision. Another test that can be done is that when we augment the strength of the transverse potential, which is associated to the hyperfine interaction within the formalism used, the ratio r increases (see for example the calculated masses for the set IV in Table II). This suggests that any deviation from $r = 1$ depends on the hyperfine interaction, in consonance with the conclusions of Ref. [15].

TABLE VI: Ratio r defined in Eq. (21) for lowest-lying and radially-excited P -wave B_c states reported in Fig. 2.

n	1	2	3	4	5
r	1.0047	1.0031	1.0021	1.0014	1.0008

As a final remark, this effective approach with a small number of parameters allows us construct the general aspects of the bottom-charmed spectrum. Our predicted energy levels are in fair agreement with other predictions, providing a guide to the experimental search for the unobserved B_c mesons.

IV. CONCLUDING REMARKS

The purpose of this work has been the investigation of the B_c meson spectrum by employing a different formalism with respect to the preceding analyses. The framework employed has been an effective version of the Coulomb gauge QCD and many-body techniques associated to the Tamm-Dancoff approximation (TDA). The interactions between quarks (quasiparticles) and antiquarks (antiquasiparticles) have been given by the sum of an improved confining potential and a transverse hyperfine interaction with an Yukawa-type kernel, being interpreted as the exchange of a constituent gluon.

Making use of a small number of parameters (dynamical mass of a constituent gluon m_g , current quark masses m_b, m_c and the magnitude of the transverse potential C_h), this approach has allowed us to analyze the basic features of B_c mesons. The calculated masses

have been optimized in order to fit them to the observed states by means of tuning of the parameters. Besides, the estimations of expected but yet-unobserved states are approximately in accordance with other findings in the literature using distinct formalisms. In particular, our calculations yield the mass for $B_c(2S)$ lighter than for $B_c^*(2S)$, which coincides with the other theoretical expectations, but not with the CMS and LHCb results at the present moment. One expects that future findings will show that the true $B_c^*(2S)$ peak must be at a higher mass as the photon emitted in the $B_c^{*+} \rightarrow B_c^+ \gamma$ radiative transition can be reconstructed.

Another aspect regarded has been the mass relation between the ground states and their radial excited states in the (n, M^2) and (J, M^2) planes. The nonlinearity is more pronounced in the (n, M^2) plane, due to the high excitation number used. The parent trajectories (beginning from the ground states) reveal a nonlinear nature more evident than the daughter trajectories (incorporating both radially and orbitally excited states), which is in qualitative accordance with other works exploring quarkonia states and mesons.

Further, the hyperfine splitting of both S and P -wave states has been studied. In both cases, we found that these splittings decrease for higher excited states but become larger as the parameter C_h grows, as expected, since it drives the strength of the term associated to the hyperfine interaction. In the case of P -wave states, the mass relation in Eq. (21) has relative theoretical errors for the lowest-lying and radially-excited states lower than 0.5%. So, this framework engenders a reasonable precision for this mass relation involving the P -wave states.

Hence, we believe that this effective approach with a minimal number of parameters is capable of offering the general aspects of the bottom-charmed spectrum, in fair agreement with other predictions. At last, all these works provide a guide to the experimental search for the unobserved B_c mesons. Some obvious extensions that deserve future studies are calculations and predictions on radiative and strong transitions and also on hybrid meson spectrum.

Acknowledgments

We are grateful to Felipe J. Llanes-Estrada for support and discussions. We also would like to thank the Brazilian funding agencies for their financial support: CNPq (L.M.A.: con-

tracts 308088/2017-4 and 400546/2016-7) and FAPESB (L.M.A.: contract INT0007/2016; F.M.C.J.: contract BOL2388/2017).

Appendix A: Wave functions of TDA equation of motion

In this Appendix we present explicitly the B_c meson spin-orbital wave functions, in terms of L, S, J (helicity indices are not displayed):

- pseudoscalar ($L = 0; S = 0; J = 0$),

$$\psi(0^-) = \sqrt{\frac{1}{4\pi}} \frac{i\sigma^2}{\sqrt{2}}, \quad (\text{A1})$$

- scalar ($L = 1; S = 1; J = 0$),

$$\psi(0^+) = -\sqrt{\frac{1}{4\pi}} (\boldsymbol{\sigma} \cdot \hat{\mathbf{k}}) \frac{i\sigma^2}{\sqrt{2}}, \quad (\text{A2})$$

- vector ($L = 0; S = 1; J = 1$),

$$\psi(1^-) = \sqrt{\frac{3}{4\pi}} \boldsymbol{\sigma} \frac{i\sigma^2}{\sqrt{2}}, \quad (\text{A3})$$

- axial ($L = 1; S = 0; J = 1$),

$$\psi(1^+) = i\sqrt{\frac{3}{4\pi}} \hat{\mathbf{k}} \frac{i\sigma^2}{\sqrt{2}}, \quad (\text{A4})$$

- axial ($L = 1; S = 1; J = 1$),

$$\psi(1^{+'}) = -i\sqrt{\frac{3}{8\pi}} (\boldsymbol{\sigma} \times \hat{\mathbf{k}}) \frac{i\sigma^2}{\sqrt{2}}, \quad (\text{A5})$$

- Tensor ($L = 1; S = 1; J = 2$),

$$\psi(2^+) = \sqrt{\frac{3}{4\pi}} \boldsymbol{\sigma} \hat{\mathbf{k}} \frac{i\sigma^2}{\sqrt{2}}, \quad (\text{A6})$$

- Pseudotensor ($L = 2; S = 0; J = 2$),

$$\psi(2^-) = \sqrt{\frac{5}{4\pi}} \hat{\mathbf{k}} \hat{\mathbf{k}} \frac{i\sigma^2}{\sqrt{2}}, \quad (\text{A7})$$

- Pseudotensor ($L = 2; S = 1; J = 2$),

$$\psi(2^{-'}) = -\sqrt{\frac{5}{4\pi}} (\boldsymbol{\sigma} \times \hat{\mathbf{k}}) \hat{\mathbf{k}} \frac{i\sigma^2}{\sqrt{2}}, \quad (\text{A8})$$

The factor ($i\sigma^2$) is introduced in order to use the same convention of Ref. [46].

Appendix B: Kernels of TDA equation of motion

Here we set out the relevant kernels obtained for the mesons described by the wavefunctions given by Eqs. (A1)-(A8):

- pseudoscalar ($L = 0; S = 0; J = 0$),

$$K^{(0^-)}(k, q) = V_1(a_5 + a_6) + V_0(a_7 + a_8) + 2U_0(a_1 + a_2) - 2W_0(a_3 + a_4); \quad (\text{B1})$$

- scalar ($L = 1; S = 1; J = 0$),

$$K^{(0^+)}(k, q) = V_0(a_5 + a_6) + V_1(a_7 + a_8) - 2U_0(a_3 + a_4) + (U_1 + W_0 - kqZ_0)(a_1 + a_2); \quad (\text{B2})$$

- vector ($L = 0; S = 1; J = 1$),

$$K^{(1^-)}(k, q) = \frac{1}{3}[3V_1(a_5 + a_6) + a_8(4V_2 - V_0) + 3a_7V_0 - 2(a_1 + a_2)U_0 + 2(a_3 + a_4)U_1 + 2qk(a_3 + a_4)Z_0 + 4(a_1k^2 + a_2q^2)Z_0]; \quad (\text{B3})$$

- axial ($L = 1; S = 0; J = 1$),

$$K^{(1^+)}(k, q) = (a_5 + a_6)V_2 + (a_7 + a_8)V_1 + 2(a_1 + a_2)U_1 - 2(a_3 + a_4)W_1; \quad (\text{B4})$$

- axial ($L = 1; S = 1; J = 1$),

$$K^{(1^{+'})}(k, q) = \frac{1}{2}(V_0 + V_2)(a_5 + a_6) + \frac{1}{2}(U_0 + U_2 - 2W_1)(a_3 + a_4) + V_1(a_7 + a_8) + Z_1(a_1k^2 + a_2q^2) + Z_0\frac{1}{2}(k^2 - q^2)(a_4 - a_3). \quad (\text{B5})$$

- Tensor ($L = 1; S = 1; J = 2$),

$$K^{(2^+)}(k, q) = \frac{1}{2}(3V_2 - V_0)(a_5 + a_6) + V_1a_7 + \frac{1}{5}(12V_3 - 7V_1)a_8 + \frac{1}{5}(U_1 - 5W_0 - 10kqZ_0)(a_1 + a_2) + \frac{12}{5}Z_1(a_1k^2 + a_2q^2) + \frac{1}{10}(27U_2 - 15W_1 - 9kqZ_1 - 4U_0)(a_3 + a_4); \quad (\text{B6})$$

- Pseudotensor ($L = 2; S = 0; J = 2$),

$$K^{(2^-)}(k, q) = \frac{1}{2}(3V_3 - V_1)(a_5 + a_6) + \frac{1}{2}(3V_2 - V_0)(a_7 + a_8) \\ + (3U_2 - U_0)(a_1 + a_2) + (3W_2 - W_0)(a_3 + a_4); \quad (\text{B7})$$

- Pseudotensor ($L = 2; S = 1; J = 2$),

$$K^{(2^{-'})}(k, q) = V_3(a_5 + a_6) + \frac{1}{2}(3V_2 - V_0)(a_7 + a_8) \\ + kqZ_1(a_1 + a_2) + \frac{1}{2}(2Z_2 - Z_0)(a_3 + a_4); \quad (\text{B8})$$

where the coefficients a_i are given by

$$a_1 = \sqrt{1 + s_k^b} \sqrt{1 + s_k^c} \sqrt{1 - s_q^b} \sqrt{1 - s_q^c}, \\ a_2 = \sqrt{1 - s_k^b} \sqrt{1 - s_k^c} \sqrt{1 + s_q^b} \sqrt{1 + s_q^c}, \\ a_3 = \sqrt{1 + s_k^b} \sqrt{1 - s_k^c} \sqrt{1 - s_q^b} \sqrt{1 + s_q^c}, \\ a_4 = \sqrt{1 - s_k^b} \sqrt{1 + s_k^c} \sqrt{1 + s_q^b} \sqrt{1 - s_q^c}, \\ a_5 = \sqrt{1 + s_k^b} \sqrt{1 - s_k^c} \sqrt{1 + s_q^b} \sqrt{1 - s_q^c}, \\ a_6 = \sqrt{1 - s_k^b} \sqrt{1 + s_k^c} \sqrt{1 - s_q^b} \sqrt{1 + s_q^c}, \\ a_7 = \sqrt{1 + s_k^b} \sqrt{1 + s_k^c} \sqrt{1 + s_q^b} \sqrt{1 + s_q^c}, \\ a_8 = \sqrt{1 - s_k^b} \sqrt{1 - s_k^c} \sqrt{1 - s_q^b} \sqrt{1 - s_q^c}. \quad (\text{B9})$$

The functions $s_{k(q)}^b$ and $s_{k(q)}^c$ are dependent of the respective gap angle obtained by solving the gap equation for the b and c quarks, respectively. Besides the functions V_n , U_n and W_n , defined in Eqs. (10) and (11), the auxiliary Z -function has been also introduced:

$$Z(|\mathbf{k} - \mathbf{q}|) \equiv U(|\mathbf{k} - \mathbf{q}|) \frac{1 - x^2}{|\mathbf{k} - \mathbf{q}|^2}. \quad (\text{B10})$$

-
- [1] F. Abe *et al.* [CDF], Phys. Rev. Lett. **81**, 2432-2437 (1998) doi:10.1103/PhysRevLett.81.2432 [arXiv:hep-ex/9805034 [hep-ex]].
- [2] V. Abazov *et al.* [D0], Phys. Rev. Lett. **101**, 012001 (2008) doi:10.1103/PhysRevLett.101.012001 [arXiv:0802.4258 [hep-ex]].

- [3] R. Aaij *et al.* [LHCb], Phys. Rev. Lett. **109**, 232001 (2012)
doi:10.1103/PhysRevLett.109.232001 [arXiv:1209.5634 [hep-ex]].
- [4] M. Tanabashi *et al.* [Particle Data Group], Phys. Rev. D **98**, no. 3, 030001 (2018).
doi:10.1103/PhysRevD.98.030001
- [5] G. Aad *et al.* [ATLAS], Phys. Rev. Lett. **113**, no.21, 212004 (2014)
doi:10.1103/PhysRevLett.113.212004 [arXiv:1407.1032 [hep-ex]].
- [6] A. M. Sirunyan *et al.* [CMS], Phys. Rev. Lett. **122**, no.13, 132001 (2019)
doi:10.1103/PhysRevLett.122.132001 [arXiv:1902.00571 [hep-ex]].
- [7] R. Aaij *et al.* [LHCb], Phys. Rev. Lett. **122**, no.23, 232001 (2019)
doi:10.1103/PhysRevLett.122.232001 [arXiv:1904.00081 [hep-ex]].
- [8] E. J. Eichten and C. Quigg, Phys. Rev. D **49**, 5845-5856 (1994) doi:10.1103/PhysRevD.49.5845
[arXiv:hep-ph/9402210 [hep-ph]].
- [9] A. P. Monteiro, M. Bhat and K. B. Vijaya Kumar, Int. J. Mod. Phys. A **32**, no.04, 1750021
(2017) doi:10.1142/S0217751X1750021X [arXiv:1607.07594 [hep-ph]].
- [10] A. P. Monteiro, M. Bhat and K. B. Vijaya Kumar, Phys. Rev. D **95**, no.5, 054016 (2017)
doi:10.1103/PhysRevD.95.054016 [arXiv:1608.05782 [hep-ph]].
- [11] N. R. Soni, B. R. Joshi, R. P. Shah, H. R. Chauhan and J. N. Pandya, Eur. Phys. J. C **78**,
no.7, 592 (2018) doi:10.1140/epjc/s10052-018-6068-6 [arXiv:1707.07144 [hep-ph]].
- [12] N. Akbar, M. Atif Sultan, B. Masud and F. Akram, Eur. Phys. J. A **55**, no.5, 82 (2019)
doi:10.1140/epja/i2019-12735-1 [arXiv:1811.07552 [hep-ph]].
- [13] E. J. Eichten and C. Quigg, Phys. Rev. D **99**, no.5, 054025 (2019)
doi:10.1103/PhysRevD.99.054025 [arXiv:1902.09735 [hep-ph]].
- [14] Q. Li, M. S. Liu, L. S. Lu, Q. F. Lu, L. C. Gui and X. H. Zhong, Phys. Rev. D **99**, no.9,
096020 (2019) doi:10.1103/PhysRevD.99.096020 [arXiv:1903.11927 [hep-ph]].
- [15] L. Chang, M. Chen, X. q. Li, Y. x. Liu and K. Raya, [arXiv:1912.08339 [nucl-th]].
- [16] P. G. Ortega, J. Segovia, D. R. Entem and F. Fernandez, Eur. Phys. J. C **80**, no.3, 223 (2020)
doi:10.1140/epjc/s10052-020-7764-6 [arXiv:2001.08093 [hep-ph]].
- [17] S. Godfrey and N. Isgur, Phys. Rev. D **32**, 189 (1985). doi:10.1103/PhysRevD.32.189
- [18] J. Zeng, J. W. Van Orden and W. Roberts, Phys. Rev. D **52**, 5229-5241 (1995)
doi:10.1103/PhysRevD.52.5229 [arXiv:hep-ph/9412269 [hep-ph]].
- [19] S. N. Gupta and J. M. Johnson, Phys. Rev. D **53**, 312-314 (1996)

- doi:10.1103/PhysRevD.53.312 [arXiv:hep-ph/9511267 [hep-ph]].
- [20] D. Ebert, R. N. Faustov and V. O. Galkin, Phys. Rev. D **67**, 014027 (2003) doi:10.1103/PhysRevD.67.014027 [arXiv:hep-ph/0210381 [hep-ph]].
- [21] S. M. Ikhdaïr and R. Sever, Int. J. Mod. Phys. A **19**, 1771-1792 (2004) doi:10.1142/S0217751X0401780X [arXiv:hep-ph/0310295 [hep-ph]].
- [22] S. Godfrey, Phys. Rev. D **70**, 054017 (2004) doi:10.1103/PhysRevD.70.054017 [arXiv:hep-ph/0406228 [hep-ph]].
- [23] S. S. Gershtein, V. V. Kiselev, A. K. Likhoded and A. V. Tkabladze, Phys. Rev. D **51**, 3613-3627 (1995) doi:10.1103/PhysRevD.51.3613 [arXiv:hep-ph/9406339 [hep-ph]].
- [24] T. Aliev, T. Barakat and S. Bilmis, doi:10.1016/j.nuclphysb.2019.114726 [arXiv:1905.11750 [hep-ph]].
- [25] Z. G. Wang, Eur. Phys. J. A **49**, 131 (2013) doi:10.1140/epja/i2013-13131-7 [arXiv:1203.6252 [hep-ph]].
- [26] I. F. Allison, C. T. H. Davies, A. Gray, A. S. Kronfeld, P. B. Mackenzie, J. N. Simone, Phys. Rev. Lett. **94**, 172001 (2005) doi:10.1103/PhysRevLett.94.172001 [arXiv:hep-lat/0411027 [hep-lat]].
- [27] R. J. Dowdall, C. T. H. Davies, T. C. Hammant and R. R. Horgan, Phys. Rev. D **86**, 094510 (2012) doi:10.1103/PhysRevD.86.094510 [arXiv:1207.5149 [hep-lat]].
- [28] N. Mathur, M. Padmanath and S. Mondal, Phys. Rev. Lett. **121**, no.20, 202002 (2018) doi:10.1103/PhysRevLett.121.202002 [arXiv:1806.04151 [hep-lat]].
- [29] M. Chen, L. Chang and Y. X. Liu, Phys. Rev. D **101**, no.5, 056002 (2020) doi:10.1103/PhysRevD.101.056002 [arXiv:2001.00161 [hep-ph]].
- [30] A. Szczepaniak, E. S. Swanson, C. R. Ji and S. R. Cotanch, Phys. Rev. Lett. **76**, 2011-2014 (1996) doi:10.1103/PhysRevLett.76.2011 [arXiv:hep-ph/9511422 [hep-ph]].
- [31] S. Cotanch, A. Szczepaniak, E. Swanson and C. Ji, Nucl. Phys. A **631**, 640C-643C (1998) doi:10.1016/S0375-9474(98)00082-7
- [32] F. J. Llanes-Estrada and S. R. Cotanch, Phys. Rev. Lett. **84**, 1102 (2000) doi:10.1103/PhysRevLett.84.1102.
- [33] A. P. Szczepaniak and E. S. Swanson, Phys. Rev. D **65**, 025012 (2001) doi:10.1103/PhysRevD.65.025012.
- [34] F. J. Llanes-Estrada and S. R. Cotanch, Nucl. Phys. A **697**, 303 (2002) doi:10.1016/S0375-

- 9474(01)01237-4 [hep-ph/0101078].
- [35] N. Ligterink and E. S. Swanson, Phys. Rev. C **69**, 025204 (2004) doi:10.1103/PhysRevC.69.025204 [hep-ph/0310070].
- [36] F. J. Llanes-Estrada, S. R. Cotanch, A. P. Szczepaniak and E. S. Swanson, Phys. Rev. C **70**, 035202 (2004) doi:10.1103/PhysRevC.70.035202 [hep-ph/0402253].
- [37] F. J. Llanes-Estrada, P. Bicudo and S. R. Cotanch, Phys. Rev. Lett. **96**, 081601 (2006) doi:10.1103/PhysRevLett.96.081601.
- [38] A. P. Szczepaniak and P. Krupinski, Phys. Rev. D **73**, 034022 (2006) doi:10.1103/PhysRevD.73.034022 .
- [39] I. J. General, P. Wang, S. R. Cotanch and F. J. Llanes-Estrada, Phys. Lett. B **653**, 216-223 (2007) doi:10.1016/j.physletb.2007.08.015 [arXiv:0707.1286 [hep-ph]].
- [40] P. Guo, A. P. Szczepaniak, G. Galata, A. Vassallo and E. Santopinto, Phys. Rev. D **77**, 056005 (2008) doi:10.1103/PhysRevD.77.056005 [arXiv:0707.3156 [hep-ph]].
- [41] P. Guo, A. P. Szczepaniak, G. Galata, A. Vassallo and E. Santopinto, Phys. Rev. D **78**, 056003 (2008) doi:10.1103/PhysRevD.78.056003 [arXiv:0807.2721 [hep-ph]].
- [42] J. M. Torres-Rincon and F. J. Llanes-Estrada, Phys. Rev. Lett. **105**, 022003 (2010) doi:10.1103/PhysRevLett.105.022003;
- [43] W. Xie, L. Mo, P. Wang and S. R. Cotanch, Phys. Lett. B **725**, 148-152 (2013) doi:10.1016/j.physletb.2013.07.003 [arXiv:1302.5737 [hep-ph]].
- [44] P. Guo, T. Yepez-Martinez and A. P. Szczepaniak, Phys. Rev. D **89**, no.11, 116005 (2014) doi:10.1103/PhysRevD.89.116005 [arXiv:1402.5863 [hep-ph]].
- [45] D. Amor-Quiroz, T. Yepez-Martinez, P. Hess, O. Civitarese and A. Weber, Int. J. Mod. Phys. E **26**, no.12, 1750082 (2017) doi:10.1142/S0218301317500823 [arXiv:1704.01947 [nucl-th]].
- [46]
- [46] L. M. Abreu, A. G. Favero, F. J. Llanes-Estrada and A. G. Sánchez, Phys. Rev. D **100**, no. 11, 116012 (2019) doi:10.1103/PhysRevD.100.116012 [arXiv:1908.11154 [hep-ph]].
- [47] L. M. Abreu, F. M. da Costa Júnior and A. G. Favero, Phys. Rev. D **101**, no.11, 116016 (2020) doi:10.1103/PhysRevD.101.116016 [arXiv:2004.10736 [hep-ph]].
- [48] H. G. Blundell, S. Godfrey and B. Phelps, Phys. Rev. D **53**, 3712 (1996) doi:10.1103/PhysRevD.53.3712 [hep-ph/9510245].
- [49] A. T. Lytle, C. T. H. Davies, D. Hatton, G. P. Lepage, C. Sturm, Phys. Rev. D **98**, no.1,

- 014513 (2018) doi:10.1103/PhysRevD.98.014513 [arXiv:1805.06225 [hep-lat]].
- [50] D. Hatton, C. Davies, B. Galloway, J. Koponen, G. Lepage and A. Lytle, [arXiv:2005.01845 [hep-lat]].
- [51] K. W. Wei and X. H. Guo, Phys. Rev. D **81**, 076005 (2010). doi:10.1103/PhysRevD.81.076005
- [52] D. Ebert, R. N. Faustov and V. O. Galkin, Eur. Phys. J. C **71**, 1825 (2011) doi:10.1140/epjc/s10052-011-1825-9 [arXiv:1111.0454 [hep-ph]].
- [53] J. K. Chen, Eur. Phys. J. C **78** (2018) no.3, 235. doi:10.1140/epjc/s10052-018-5718-z
- [54] J. K. Chen, Phys. Lett. B **786**, 477 (2018) doi:10.1016/j.physletb.2018.10.022 [arXiv:1807.11003 [hep-ph]].
- [55] D. Jia and W. C. Dong, Eur. Phys. J. Plus **134**, no. 3, 123 (2019) doi:10.1140/epjp/i2019-12474-8 [arXiv:1811.04214 [hep-ph]].
- [56] A. V. Anisovich, V. V. Anisovich and A. V. Sarantsev, Phys. Rev. D **62**, 051502(R) (2000) doi:10.1103/PhysRevD.62.051502 [hep-ph/0003113].
- [57] A. V. Anisovich *et al.*, Phys. Lett. B **491**, 47 (2000) doi:10.1016/S0370-2693(00)01018-2 [arXiv:1109.0883 [hep-ex]].
- [58] S. S. Afonin, Phys. Rev. C **76**, 015202 (2007) doi:10.1103/PhysRevC.76.015202 [arXiv:0707.0824 [hep-ph]].
- [59] C. Peset, A. Pineda and J. Segovia, Phys. Rev. D **98**, no.9, 094003 (2018) doi:10.1103/PhysRevD.98.094003 [arXiv:1809.09124 [hep-ph]].
- [60] In Ref. [15] is argued that there should be possible hidden symmetry or an underlying principle that makes this relation valid for the P -level of charmonium and bottomonium systems, but also for the case of unequal-flavor case, like the the B_c family.